Atmos. Meas. Tech. Discuss., 5, 3645–3692, 2012
www.atmos-meas-tech-discuss.net/5/3645/2012/
doi:10.5194/amtd-5-3645-2012

Atmospheric Measurement Techniques Discussions

Assessment of a multi-species in-situ FTIR for precise atmospheric greenhouse gas observations

S. Hammer[1], D. W. T. Griffith[2], G. Konrad[1], S. Vardag[1], C. Caldow[2], and I. Levin[1]

[1]Institut für Umweltphysik, Heidelberg University, Germany
[2]School of Chemistry, University of Wollongong, Australia

Received: 27 March 2012 – Accepted: 26 April 2012 – Published: 22 May 2012

Correspondence to: S. Hammer (shammer@iup.uni-heidelberg.de)

Published by Copernicus Publications on behalf of the European Geosciences Union.

Abstract

We thoroughly evaluate the performance of a multi-species, in-situ FTIR analyser with respect to high accuracy needs for greenhouse gas monitoring networks. The in-situ FTIR analyser measures CO_2, CO, CH_4 and N_2O mole fractions continuously, all with better reproducibility than requested by the WMO-GAW inter-laboratory compatibility (ILC) goal. Simultaneously determined $\delta^{13}CO_2$ reaches reproducibility as good as 0.03‰. This paper focuses on the quantification of residual dependencies between the measured components and the thermodynamic properties of the sample as well as the cross-sensitivities among the sample constituents. The instrument has proven to be linear for all components in the ambient range. The temporal stability of the instrument was investigated by 10 months of continuously collected quality control measures. Based on these measures we conclude that for moderately stable laboratory conditions weekly calibrations of the instrument are sufficient to reach WMO-GAW ILC goals.

1 Introduction

The globally distributed in-situ greenhouse gas (GHG) monitoring network is one of the mainstays of modern climate research. Only a few continuous atmospheric CO_2 records go back to the 1950s (Keeling et al., 1976) but nowadays many stations monitor nearly all long-lived GHGs with in-situ instrumentation (Worthy, 2003; Messager et al., 2008). The required accuracy and precision of the most important GHG species have been set to such limits that allow extracting the required biogeochemical information from spatial differences which are needed for quantifying continental scale GHG fluxes and their inter-annual changes (WMO report No. 5, 1981, cited in Francey and Steele, 2003). Over the most recent decades, non-dispersive infrared (NDIR) analysis of CO_2 and gas chromatography (GC) of CO_2 and all other long-lived GHGs has been proven to provide this accuracy and precision; they have thus become standard techniques for GHG monitoring. Both techniques require special care, maintenance,

AMTD
5, 3645–3692, 2012

frequent calibration and quality control measures to verify data quality; they are thus labour-intensive in their day-to-day operation. In recent years, optical techniques like Cavity Ring Down Spectroscopy (CRDS), Off-Axis Integrated Cavity Output Spectroscopy (OA-ICOS) or Fourier Transform Infrared Spectroscopy (FTIR) have reached similar or even better precision than traditional GC systems. Contrary to the discrete samples measured with GC systems, these techniques offer real continuous data acquisition and are in general less labour intensive (Winderlich et al., 2010). Another benefit of optical spectroscopy is the possibility of discriminating isotopologues, e.g. it allows for continuous measurement of $\delta^{13}CO_2$. The challenge of isotopologue-selective measurements is, however, to accurately determine the absolute sums of all individual isotopologues. To do so, either all relevant isotopologues have to be measured independently, as done by the in-situ FTIR analyser or assumptions on the mean relation between $\delta^{13}CO_2$ and $^{12}CO_2$ in clean air have to be taken into account during evaluation and/or should be already incorporated in the calibration of the instrument (Chen et al., 2010).

Optical techniques can be divided into two fundamentally different methods: (1) laser based methods and (2) broad band infrared spectroscopy. The major distinctive feature between them is the range of the recorded and evaluated absorption spectrum. Whereas laser-based instruments are tuned to a narrow absorption window with ideally little interference from other species, the FTIR scans a broad IR range thereby offering the possibility to measure a large number of species simultaneously. Especially the laser-based techniques like CRDS and OA-ICOS have been extensively and successfully studied by the GHG measurement community; some instruments have already found their way into today's observational networks (Winderlich et al., 2010).

So far, studies discussing the use of the in-situ FTIR technique for GHG monitoring purposes are rare although promising (Griffith et al., 2010). Therefore detailed investigations of the potential and the possible shortcomings of this technique with respect to the accuracy goals set by WMO/GAW experts for clean background air monitoring should be performed before it is used widely within the monitoring

AMTD
5, 3645–3692, 2012

community. Especially questions regarding long-term stability, calibration frequency and cross-sensitivity of different trace gases have to be addressed. In the present paper we report on detailed experiments which were performed at the Institut für Umweltphysik (IUP), Heidelberg University on instrument repeatability, parameter- and cross-sensitivity, linearity and long-term stability of an in-situ FTIR analyser which was designed and built at the University of Wollongong, Australia (UOW) (Griffith et al., 2012). These data have been gathered in the IUP laboratory as well as in the course of the ICOS (Integrated Carbon Observation System, http://www.icos-infrastructure.eu/) demo-experiment where the instrument was run at two remote stations in Europe. The UOW FTIR instrument is subject to an ongoing development process and many findings of this paper have already led to improvements in newer instrument versions. Nonetheless, our findings are generally applicable to any in-situ FTIR instrument and can therefore be used as a guideline for in-situ FTIR users in order to raise awareness for high-end accuracy applications.

In the first part of the paper we briefly describe the instrumental setup and investigate the performance of the instrument as it was used during the first year as well as results of the ICOS demo-experiment. In the last section we will then briefly outline the improvements and their benefits which were achieved based on the main findings of this paper.

2 Instrumental setup and sample handling

Griffith et al. (2010, 2012) describe the improved in-situ FTIR instrument used in the present work which is based on the early version of the instrument as described by Esler et al. (2000a, b). Further on we will refer to the instrument as the "in-situ FTIR analyser". The essential parts of the in-situ FTIR analyser (Griffith et al., 2010, 2012) and the modifications introduced in Heidelberg for the first year and in the course of the ICOS demo-experiment are presented. In anticipation of the last section, the hardware modification resulting from the first year's findings are introduced as well.

AMTD
5, 3645–3692, 2012

2.1 Instrument components and sample handling

The instrument consists of a commercially available FTIR interferometer (IRcube, Bruker Optics, Germany) and a 3.5 l multi-pass cell with 24 m optical path length (PA-24, InfraredAnalysis, Anaheim, USA) (see Fig. 1 for the Heidelberg set-up). To avoid artefacts, the transfer-optics between the interferometer and the multi-pass cell as well as the interferometer housing itself are permanently flushed with high purity nitrogen (5.0). The multi-pass cell is equipped with an in-situ PT100 resistance temperature detector (RTD) and with a pressure sensor (HPM-760s, Teledyne Hastings, USA). The FTIR interferometer and the multi-pass cell are aligned via an optical bench situated in an actively temperature controlled enclosure. In its basic configuration the in-situ FTIR analyser has four separate sample inlets and air is drawn through the instrument using an oil-free vacuum pump (model MV2NT, Vacuubrand, Germany) at the outlet of the instrument. More intake lines can be added via a multi-position valve (MWSD16 selection valve, Valco, USA).

The in-situ FTIR analyser has a built-in sample drying system consisting of a 24 inch Nafion dryer (Permapure, Toms River, NJ, USA) operated in counter-flow mode, followed by a chemical dryer filled with $Mg(ClO_4)_2$ for uptake of residual water. The drying system reaches a dew point of $\approx -65\,^{\circ}C$ and can be by passed if measurement of H_2O isotopologues is of interest. Sample flow through the system was initially adjusted with a needle valve (NV) and monitored using a flowmeter (FM) mounted at the outlet of the cell. For additional stabilization of the sample properties (e.g. temperature and pressure) in the cell the Heidelberg configuration used an add-on external mass flow-controller (MFC) (2 slpm, MKS Instruments, USA) in between the outlet of the multi-port valve and the instrument air inlet. In the current, modified configuration of the in-situ FTIR the sample flow through the cell is only controlled by a built-in mass flow-controller (Model 3660, Kofloc, Japan), replacing the needle-valve flowmeter unit as well as our add-on external flow-controller. In the new Heidelberg set-up the sample

AMTD
5, 3645–3692, 2012

pressure in the cell is additionally controlled by an electronic pressure controller (EPC) (P-602CV EL-Press, Bronkhorst, The Netherlands) mounted at the cell inlet.

In the Heidelberg setting the cell is operated at slight overpressure to increase signal-to-noise ratio and to ease leak detection. A diaphragm pump fitted with an EPDM membrane (N 86 KN.18, KNF Neuberger, Germany) is used to pressurize ambient air up to 1800 hPa. Long-term GC experience has shown that these pumps have negligible effects on the measured species. Nevertheless each pump is tested for contamination prior to its use.

2.2 Spectroscopic concentration retrieval

The spectral range of the IRcube is 1800–7500 cm^{-1} with a 1 cm^{-1} resolution. The UOW FTIR analyzer records and stores a broadband absorption spectrum from 1800–5000 cm^{-1} for each measurement. The recorded spectra are analysed online by non-linear least squares fitting of sections of the measured spectrum with a modelled spectrum calculated from the HITRAN database of absorption line parameters (Rothman et al., 2005). The theoretical spectrum is calculated by MALT (Multiple Atmospheric Layer Transmission) as described elsewhere (Griffith, 1996; Griffith et al., 2012). Three separate spectral regions are fitted for each spectrum: 2150–2320 cm^{-1} for $^{13}CO_2$, $^{12}CO_2$, CO and N_2O, 3001–3150 cm^{-1} for CH_4 and 3520–3775 cm^{-1} for CO_2 (all isotopologues) and residual H_2O. The spectral analysis determines the molar concentrations (c_i (mol m^{-3})) of each gas species. To convert molar concentrations into mole fractions (x_i (mol mol^{-1})), sample pressure and temperature need to be taken into account:

$$x_{i(\text{wet})} = \frac{c_i}{\left(\frac{p}{RT}\right)} \quad (1)$$

where p is the absolute cell pressure, T the absolute temperature, R the Universal Gas Constant and i the investigated species. Since residual water is determined for each sample, dry air mole fractions x_i can easily be derived from:

AMTD
5, 3645–3692, 2012

$$x_{i(\mathrm{dry})} = \frac{x_{i(\mathrm{wet})}}{(1 - x_{\mathrm{H_2O}})} \quad (2)$$

2.3 Standard Operating Conditions

In the Standard Operating Conditions (SOC) the compartment temperature is set to 30.0 °C. It is stable within ±0.06 °C, which leads to a stability of the cell-temperature of ±0.02 °C for moderately stable laboratory conditions ±1 °C. All samples are dried using the built-in drying system (Fig. 1). We chose to flush both sample types, ambient air and tank air, continuously through the cell with the same flow rate of 1 ± 0.02 slpm. This approach was taken to assure comparability for ambient air and calibration gas measurements. In the original instrumental set-up the cell pressure could be set via sample delivery pressure and sample flow rate and was kept at 1100 ± 8 hPa in Standard Operating Conditions. With the modified set-up sample pressure and flow are controlled separately to better than 0.01 % (pressure) and 0.8 % (flow). The measurement interval is set to 3 min, from which a 2.5 min spectra collection period is followed by 0.5 min online analysis. This was chosen as a compromise between instrument precision (increasing with averaging time), smoothing-out natural variability in the sampled air which itself blurs the averaged spectra, and the approximately 3-min exchange time for gas in the cell at 1 slpm flow rate. However, measurements of ambient air and high pressure cylinder samples (i.e. calibration gases) differ with respect to the sample injection and cell history. Under SOC each sample switch-over, i.e. changing from continuous ambient to cylinder measurements and vice versa, involves a two-step evacuation of the cell which is described in detail in Sect. 2.4. Possible disadvantages of evacuating the cell, i.e. by disturbance of moisture or temperature equilibrium, will be discussed later on. In the SOC each cylinder or calibration gas measurement was performed over 30 min including the sample change-over and requires a total gas volume of about 27 l of air.

AMTD
5, 3645–3692, 2012

2.4 Sample exchange and thermodynamic equilibrium in the cell

Measurement accuracy depends on the instrument's performance but also on the ability of completely exchanging the sample in the cell without memory effects. Thus, the cell has to be either evacuated or flushed for a sufficiently long time to completely remove the previous sample. We will briefly discuss both approaches:

a. Flushing: the mean exchange time τ of a well mixed volume is given by the ratio of volume to flow-rate. The influence of the preceding sample decreases according to $\exp(-t/\tau)$ where t is the flushing time. Thus, we need more than $t = 8\tau$ to reduce the memory effect to less than 0.03 %, which in case of a 100 µmol mol^{-1} change in CO_2 between the two samples results in 0.03 µmol mol^{-1} memory effect. With the given cell volume and the standard flow rate of 1 slpm, a flushing time of 28 min is thus theoretically required. An example of this change-over method is illustrated in Fig. 2 (black squares). In this example the equilibrium value, which is defined as the average mole fraction measured from minute 30 to 45 is reached after 21 min with a mole fraction difference between the two samples of 140 µmol mol^{-1}.

b. Evacuation: to reach comparably small memory effects as under (a), the cell and the inlet system need to be evacuated to <0.3 hPa, which, with the available equipment, is not reached within 30 min. Thus, we decided to use a two step evacuation procedure: the cell is first evacuated to 10 hPa, then filled with the new sample to 500 hPa, evacuated a second time down to 10 hPa and subsequently filled to the desired cell pressure of 1100 hPa. This stepwise change-over is much faster than a one-step evacuation and ensures that the memory effect is less than 0.02 %. The complete sample change-over procedure requires 7 l of gas and takes eight minutes, including one minute stabilisation after the final settings are reached. An example of the two-step evacuation procedure is also shown in Fig. 2 (blue squares).

AMTD
5, 3645–3692, 2012

Using the two-step evacuation procedure for sample exchange, close to equilibrium values are already observed 12 min after a sample change-over. As evacuation and refilling affects the temperature of the cell, the first two measurements (taken in minute 6 to 9 and 9 to 12) have to be rejected.

However, exchanging the sample entirely, and thus avoiding memory effects, is not necessarily sufficient to avoid transient settling-in effects after sample change-over. The thermodynamic properties of the sample, like temperature and pressure, need to reach their equilibrium conditions as well. Sample temperature is especially crucial, since, in contrast to pressure, we cannot assume that temperature is homogeneously distributed within the cell. This may have several causes, (a) different sample temperatures when entering the cell, (b) the spectrometer heats one end of the cell causing a small but significant temperature gradient along the cell, (c) the Reynolds number of the cell calculated for our SOC is only about 10; thus, mixing is far from turbulent, leading to a persistence of any temperature gradient.

The impact of thermodynamic disequilibrium is shown in Fig. 2 by the red squares. These measurements have been performed using the same cylinder, regulator and evacuation procedures as for the data indicated in blue, however, the cell was rotated by 180°. Turning the cell upside-down changed the position of the temperature sensor as well as that of the 1/4″ dip-tube which delivers the sample into the cell. For the measurements plotted in red the dip tube was at the top of the cell, and the temperature sensor was at the bottom. We can assume that the memory effect caused by incomplete sample exchange is similar for both positions since the same two-step evacuation approach was used. But due to the different location of the sample inlet and/or the temperature sensor the sample apparently takes longer until it reaches its thermodynamic equilibrium. Since this settling-in effect is seen for all components, it seems likely that it might be related to temperature. The measured sample temperature between the two cell positions changed by 0.5 °C; higher temperatures were observed with the temperature sensor in the upper position. Thus we can conclude that temperature is not homogeneously distributed in the cell, and that we are not able to measure the true

AMTD
5, 3645–3692, 2012

mean sample temperature with one temperature sensor only. However as long as the temperature distribution in the cell is stable under SOC and is reached for both ambient air and cylinder measurements, the calibration of the instrument will compensate for the error in temperature measurement.

3 Residual sensitivities to sample properties and inter-species cross-sensitivities

The line shapes of the investigated species are dependent on pressure- and Doppler-broadening and thus depend on sample properties like pressure and temperature. For both broadening effects temperature and pressure dependent line widths are tabulated in the HITRAN 2004 database (Rothman et al., 2005); they are considered by the FTIR spectra evaluation program MALT (Griffith, 1996), using the measured sample temperature and pressure. However, the line shape parameters themselves are subject to ongoing improvement: as an example, for the CO_2 line parameters, differences of up to a few percent are reported in recent studies (Long et al., 2011; Nakamichi et al., 2006). Small errors in the HITRAN temperature and pressure parameters and in the measured temperature and pressure lead to systematic errors in the estimated molar concentrations and may thus be the underlying cause of "residual" pressure and temperature sensitivities, which have been investigated in detail in the present work.

In addition to the residual pressure and temperature sensitivities caused by inaccuracies in the spectroscopic parameters, the conversion from molar concentrations to mole fractions (see Eq. 1) constitutes a direct link to the measured sample parameters and their precision. This emphasizes the importance of precise cell temperature and pressure measurements. Determining the average sample temperature is challenging since temperature may not be homogeneous within the cell. Currently, temperature is measured in one location only, assuming a constant temperature distribution. However, the true temperature distribution in the cell depends on the flow-rate used to flush the sample through the cell. The measured mole fractions may thus implicitly depend on

AMTD
5, 3645–3692, 2012

the flow-rate. In addition to the flow rate, the temperature distribution in the cell is sensitive to thermal pre-conditioning of the sample and the actual way in which the sample is injected into the cell. In the current FTIR setup the sample is flushed into the cell via a 1/4″ dip tube.

Apart from residual pressure, temperature and flow sensitivities, additional inter-species cross-sensitivities exist which are caused by overlapping spectral absorption regions of different trace species. Generally the MALT least squares fit is able to disentangle the contributions to absorption at each wave number and to attribute their shares to the different species. Nevertheless, the MALT algorithm, the measured spectra, and the HITRAN data are not perfect and small inter-species cross-sensitivities remain. Since H_2O absorption in the infrared region occurs at many different wavelengths, the inter-species sensitivity to residual water vapour is noticeable for all investigated species, apart from CH_4. The second strongest absorber in ambient air is CO_2. Since the $^{13}CO_2$, and N_2O absorptions in the 2150–2320 cm^{-1} region overlap with strong absorption of $^{12}CO_2$, inter-species cross-sensitivities to CO_2 do also exist.

3.1 Sensitivity experiments

We carried out a series of dedicated experiments to detect and quantify the residual sensitivities to sample properties (pressure, temperature and flow) and the cross sensitivities (H_2O and CO_2) of the in-situ FTIR analyser. If applicable, these measurements were used to define correction functions for each species. In all experiments the investigated sample property or species was systematically varied while all other parameters or species were kept as constant as possible. The experiments have been repeated several times over the course of one year to investigate temporal stability of the sensitivities. For each test we used ambient Heidelberg air collected in high pressure cylinders with a diving compressor (model P3W, Bauer, Germany) and dried to a dew-point of approximately −40 °C. The cylinders (40 l L6X aluminium, Luxfer, UK) and pressure regulators (model 14A, Scott Specialty Gases, USA) have proven to be

AMTD
5, 3645–3692, 2012

suitable for high precision GHG measurements by GC analysis (Hammer, 2008). Each cylinder filling was checked for drifts before and after use by GC analysis.

To investigate the residual sensitivities against temperature, pressure and flow, the respective parameter was tuned at the FTIR analyser itself. Determining the inter-species cross-sensitivities, involved a custom-made mixing device, consisting of two mass flow controllers (MFC) and a scrubbing agent, either Ascarite® for CO_2, or $Mg(ClO_4)_2$ for H_2O. The mixing device divides the sample stream into two branches, one of them containing the scrubbing agent. After scrubbing, both branches are re-combined and the mixed gas is injected into the in-situ FTIR analyser.

One residual sample property or cross-sensitivity experiment measures a constant sample with respect to at least four different settings of the investigated sensitivity. For each setting we allowed sufficient time to re-establish equilibrium in the whole system, i.e. until the variability in CO_2 was on the order of the instrument's repeatability and then held constant for at least 30 min. The averaged dry air mole fractions for each equilibrium setting were then used to quantify the sensitivity. In the following sections, the results of the experiments will be discussed in detail with respect to their significance and temporal stability. As reference for the required precision to monitor natural variability at clean air background sites we will refer to the inter-laboratory compatibility (ILC) goals as defined by the WMO-GAW expert group (WMO, 2011). The authors are aware that "precision" and "compatibility" are two different concepts. However, since to our knowledge no explicit precision goals for GHG measurements are defined, we use the inter-laboratory compatibility goals instead, which are as follows: 0.1 or 0.05 µmol mol^{-1} for CO_2 in the Northern, respectively the Southern Hemisphere, 0.01 ‰ for $\delta^{13}CO_2$, 2 nmol mol^{-1} for CO and CH_4 and 0.1 nmol mol^{-1} for N_2O. A compilation of all determined residual- and cross-sensitivity parameters determined for our in-situ FTIR analyser is given in Table 1.

AMTD
5, 3645–3692, 2012

3.2 Residual pressure sensitivity (RPS)

All five species, CO_2, $\delta^{13}CO_2$, CO, CH_4 and N_2O, displayed a significant residual sensitivity to cell pressure. Two different pressure ranges, one from 800 to 1200 hPa and the second from 1085 to 1115 hPa, were tested. The observed residual pressure sensitivities (RPSs) were linear and compatible for both pressure ranges as displayed in Fig. 3a for CO_2. This allows the use of a linear correction function to account for the residual pressure sensitivity. The slope of this correction function was determined by a weighted total least squares fit, accounting for errors in pressure and the investigated species (Krystek and Anton, 2007). During the year, nine RPS experiments were conducted for all species. The temporal evolution of the derived pressure sensitivity slopes for CO_2 is shown in Fig. 3b. The observed slopes vary between 0.0078 and 0.0092 ($\mu mol\,mol^{-1}\,hPa^{-1}$). The uncertainties of the slopes depend on the investigated pressure range, thus, since the RPS has proven to be linear, a larger pressure range is preferable to determine the sensitivity since the fit is more stable and the experiment is easier to conduct. Table 1 summarizes the averaged slopes and their 1σ standard deviation. For CO_2, CH_4 and N_2O the residual pressure sensitivity slopes were temporally stable within their uncertainties and had a standard deviation of 10 %. $\delta^{13}CO_2$ and CO showed a slight temporal change leading to a standard deviation of 30 % for the correction functions for these two components. To better judge the relevance of the residual sensitivities an example based on typical ranges of the investigated parameter is given in Table 1 as well. Although the additional flow controller helped to stabilise cell pressure, occasional changes in the order of ±10 hPa were observed during our measurements. If uncorrected, these pressure variations translate to 0.17 $\mu mol\,mol^{-1}$ CO_2 variations; they are thus larger than the inter-laboratory compatibility (ILC) target for CO_2. The same is true for $\delta^{13}CO_2$, and N_2O (see Table 1). All three components thus need to be corrected. The uncertainty, introduced by the residual pressure correction, is negligible for CO_2 and N_2O. In case of $\delta^{13}CO_2$ a temporal trend in the RPS leads to a larger uncertainty in the averaged correction factor. This error can be reduced

AMTD
5, 3645–3692, 2012

by introducing a temporally changing RPS correction. Nevertheless even when we assume a constant RPS the pressure introduced deviation is reduced by a factor of 2.5 compared to the uncorrected values. For CO and CH_4 the RPS corrections are smaller than the required ILCs for the assumed 10 hPa pressure change. Still, for CH_4 in contrast to CO the RPS is significant and its correction will improve the precision of the measurements. Apart from $\delta^{13}CO_2$, the stability of the correction parameters indicates that annual determination of the residual pressure sensitivity should be sufficient to take into account systematic long-term drifts of the RPSs. The underlying cause of the drift in the $\delta^{13}CO_2$ RPS correction parameter is not yet understood.

3.3 Residual temperature sensitivity (RTS)

Compared to the RPS, the residual temperature sensitivity (RTS) has the additional complication that we do not measure the *true* mean sample temperature with one temperature sensor (see Sect. 2.4). The RTD sensor was placed near the outlet of the cell whilst the later used thermocouple was located in the middle of the cell. The sample temperature distribution within the cell depends at least on three parameters, (a) the set temperature of the enclosure, (b) the sample temperature when entering the cell, (c) the sample flow-rate. In total, six dedicated RTS experiments were performed for all species. In order to investigate the RTS the temperature of the cell enclosure was varied either in its normal operational range, i.e. between 29.9 °C and 30.1 °C, or in a wider range from 29.7 °C to 30.3 °C. For each set temperature step we allowed enough time for the whole system to equilibrate. In our set-up this took roughly 60 to 90 min, based on the CO_2 variability. For CO_2, N_2O and $\delta^{13}CO_2$, linear residual temperature sensitivities were observed in each experiment. In case of CO_2, although each experiment showed good linear relations, the slopes varied substantially and even changed sign after six months. For N_2O and $\delta^{13}CO_2$ the RTS was stable within 30 % for all experiments. The residual temperature sensitivity for CO and CH_4 was weak, not temporally stable and only for some experiments a distinct relation to cell temperature was observed. The averaged RTS slopes and their standard deviations are given in Table 1.

AMTD
5, 3645–3692, 2012

For better evaluation of the results an example based on observed peak-to-peak temperature variability of 0.1 °C is listed as well. When considering the ILC targets, only the observed RTS for $\delta^{13}CO_2$ is significant and needs to be corrected.

3.4 Temperature disequilibrium sensitivity (TDS)

Residual temperature sensitivities derived in the dedicated temperature sensitivity experiments were small and not crucial to our measurement performance. However, stronger temperature sensitivities were present in our cylinder gas measurement records, implying that temperature is one of the key parameters to perform precise in-situ FTIR measurements. In the course of the ICOS demo-experiment the in-situ FTIR analyser was set-up in different laboratories under different environmental conditions, i.e. averaged laboratory temperatures ranged from 17 to 27 °C. Although the enclosure temperature was stable at 30.00 ± 0.05 °C at all locations, cell temperature varied slightly with laboratory temperature. The ambient temperature influences the sample temperature before entering the instrument as well as all parts of the in-situ FTIR analyser which are not in the temperature controlled enclosure, e.g. the drying system (see Fig. 1). Figure 4 shows the deviations from the averaged mole fraction of the daily to two-daily measured sub-target tank with respect to the cell temperature. The other three simultaneously measured cylinders, two calibration gases and the regular target gas, show similar temperature dependencies. We will further refer to this effect as the temperature disequilibrium sensitivity (TDS).

For CO_2 a linear approximation of the TDS is justified which is expressed by a correlation coefficient $r^2 = 0.97$, whereas for the other components the linear fit reaches only correlation coefficients between 0.85 and 0.95. In case of N_2O the smaller r^2 is caused by a group of outliers which are visible in CO as well. For CO a step change would be justified as well; however for sake of consistency between components and in absence of more data, we chose the linear fit. For CH_4, $\delta^{13}CO_2$ and N_2O additional systematic variation is observed between 29.4 and 29.6 °C which may be caused by some other

AMTD
5, 3645–3692, 2012

non-identified parameter. The slopes of the linear relations and their uncertainties are summarized in Table 1 as well.

The observed temperature disequilibrium sensitivities for cylinder measurements are much larger than the RTSs which were derived from the dedicated temperature experiments described in Sect. 3.3. For the typical temperature range of 0.1 °C the effect is significantly larger than the ILC goals for CO_2, $\delta^{13}CO_2$ and N_2O. A possible cause for the difference between the two temperature sensitivity results may arise from different conditions of the instrument. While in the dedicated RTS experiments sample air was continuously flushed through the cell, each cylinder measurement, performed under standard operating conditions, comprises evacuation of the cell prior to the measurement (see Sect. 2.3). This might lead to a difference in cell temperature distributions for cylinder measurements and constantly flushed measurements. The evacuation of the cell itself causes adiabatic cooling on the order of 5 °C. Although this adiabatic cooling effect is compensated for during the re-filling of the cell, it seems likely that the temperature distribution in the cell does not come to full equilibrium during the cylinder measurement and is therefore not fully comparable to continuously flushed measurements. The evacuation-induced temperature deviation is further amplified by the slow-responding RTD temperature sensor recording deviating temperatures even if the sample temperature has already settled. This was the reason why the later modifications included a replacement of the RTD sensor with a faster responding thermocouple.

In order to investigate the effect of the initial sample temperature on the cell temperature we conducted an experiment where a cylinder was first measured at room temperature before the entire cylinder was cooled to zero degrees Celsius and measured again. The cell temperature as well as the measured mole-fractions did, however, not change in this experiment. This implies that the sample pre-treatment in the in-situ FTIR analyser, i.e. the Nafion and perchlorate dryer, is sufficient to compensate for a 30 °C temperature difference. Further detailed investigations to explain the different temperature sensitivities for calibration cylinder measurements performed under SOC (Fig. 4) and continuous flow measurements is urgently needed. In our evaluation procedure we

AMTD
5, 3645–3692, 2012

used the temperature sensitivity correction parameters derived from the sub-target gas measurements (TDS) to correct all our standard and target gas measurements since they are subject to the same influences.

3.5 Flow rate sensitivity

Neither the spectroscopic nor the mole fraction determinations have a direct link to the sample flow rate through the cell. The flow rate has only an indirect effect on the temperature distribution in the cell. Thus we expect the flow rate sensitivity to be small compared to the temperature sensitivity. Nevertheless, the flow rate sensitivity was investigated in three dedicated experiments, mainly motivated from the observed difference between a constantly flushed and a closed-off cell. Apart from CO, the measured mole fractions are always higher in a closed off cell than in a constantly flushed cell. Under our standard operating conditions this effect can be as large as 0.25 µmol mol^{-1} for CO_2, 0.6 ‰ for $\delta^{13}CO_2$, −0.1 nmol mol^{-1} for CO, 1.4 nmol mol^{-1} for CH_4 and 0.28 nmol mol^{-1} for N_2O.

The observed flow sensitivity in the range between 0.8 and 1.2 slpm could be linearly approximated, however the linearity disappeared when approaching zero flow. As expected the flow sensitivities are small. In addition to this, the gas-flow through the cell was very stable due to the additional sample flow-controller. Thus the effects of the flow-sensitivity are negligible for all trace gases. For $\delta^{13}CO_2$ the flow sensitivity is larger than the ILC target; however, as the repeatability of $\delta^{13}CO_2$ measurements is still on the order ±0.03 ‰ this result is not significant.

3.6 H_2O cross-sensitivity

Measuring the H_2O cross sensitivity is experimentally challenging and time consuming since it takes time until the moisture equilibrium between gas-phase and instrument surfaces is established. The drying cartridge in the mixing device acts as an additional resistance and it was not until our last experiments that we introduced a needle valve

AMTD
5, 3645–3692, 2012

in the direct branch of the mixing device to counteract this resistance. Thus, for the first experiments the total resistance of the mixing device changes according to flow proportion in the course of the H_2O cross-sensitivity experiment. This leads to a variation in cell-pressure on the order of 10 hPa during the experiment. In the following all results have been corrected for the residual pressure sensitivity before the H_2O cross-sensitivity was determined.

A further challenge is a hysteresis effect in the H_2O cross-sensitivity which is differently pronounced for each individual species. Figure 5 shows the H_2O cross-sensitivity for N_2O and the very pronounced hysteresis effect. In contrast to the dedicated H_2O cross-sensitivity experiments performed later on, this test was conducted with gradually changing cell moisture. The H_2O cross sensitivity is linear while humidifying the cell (from red to yellow in Fig. 5), whereas a clear hysteresis appears during drying (from green to blue). The origin of the H_2O hysteresis is believed to be related to surface effects in the instrument but was not further investigated since such large moisture variations do not occur in our standard operation conditions. However they may become relevant if also water and water isotopologues shall be measured with the instrument.

For the five dedicated H_2O cross sensitivity experiments the investigated H_2O range was restricted to moisture levels between 2 and 10 µmol mol^{-1}, i.e. those which may occur during the lifetime of one $Mg(ClO_4)_2$ drying cartridge. Individual H_2O concentrations were kept as constant as possible for each set point to minimise transient effects. Within the measurement precision, no significant H_2O cross-sensitivity was observed for N_2O and $\delta^{13}CO_2$. This is explained by the weak H_2O absorption in the spectral region of N_2O, and for $\delta^{13}CO_2$ the H_2O cross sensitivity is low since all CO_2 isotopologues are subject to a similar H_2O cross-sensitivity. Although some experiments did show a clear relation between H_2O level and CH_4 or CO mole fractions, no unequivocal cross-sensitivity could be determined for these two trace gases. Only for CO_2 a more or less temporally stable H_2O cross-sensitivity was found with a 1σ standard deviation of ±50 %. The unstable results are most likely due to experimental problems. Precise adjustment and stability of moisture levels in the range between 2–10 µmol mol^{-1} is

AMTD
5, 3645–3692, 2012

difficult to achieve and in the initial set-up of the mixing device small H_2O cross sensitivities have been superimposed by cell pressure variations. Further experiments with additional means to stabilise cell pressure were needed and later on performed with the improved version of the in-situ FTIR analyser. However, since the variations in the residual moisture level during standard operating conditions can be restricted to less than 2 µmol mol^{-1} the H_2O cross-sensitivity is not very important. In Table 1 the H_2O effect is shown in an example calculation for a 2 µmol mol^{-1} effect, which exemplifies that for all species the effect is smaller than the ILC target. Nevertheless for CO_2 the H_2O cross-sensitivity is larger than the instrument's repeatability and thus worth correcting. The CO_2 variability associated with the H_2O cross-sensitivity could at least be halved by applying the H_2O correction.

3.7 CO_2 cross-sensitivity

$^{12}CO_2$ is the strongest absorber in the spectral range between 2150 and 2320 cm^{-1} and its absorption ranges do partly overlap with those of $^{13}CO_2$, N_2O and CO which are detected in the same spectral range. Since MALT uses a broad spectral region for fitting, it is able to distinguish the different species; however certain cross sensitivities to $^{12}CO_2$ remain for all mentioned species. For CH_4 the CO_2 cross-sensitivity effect is negligible since the CH_4 concentration is derived at 3001–3150 cm^{-1} where no significant $^{12}CO_2$ absorption occurs. In contrast to all previously discussed sensitivities, the influence of the CO_2 cross-sensitivity cannot be reduced by minimising the variability of the causing agent. Thus, precise determination of the CO_2 cross sensitivity is vital.

To vary the CO_2 amount we used the mixing device described above with an Ascarite (Sigma Aldrich, USA) filled cartridge. Ascarite has shown to be suitable to remove CO_2 without altering the mole fractions of the other investigated greenhouse gases (Glatzel-Mattheier, 1997). In order to use the results of the CO_2 cross-sensitivity experiment for $\delta^{13}CO_2$ as well, it is crucial to remove the CO_2 entirely in the Ascarite branch of the mixing device to avoid isotope fractionation. This was verified by taking aliquot flask

AMTD
5, 3645–3692, 2012

samples for each CO_2 level and analysing $\delta^{13}CO_2$ by mass spectrometry. For our experimental conditions with CO_2 amounts as high as 800 µmol mol^{-1} and a flow rate of up to 1 slpm, 80 g of Ascarite are sufficient to completely remove CO_2 from the Ascarite branch over the 10 h duration of the experiment.

In total seven cross-sensitivity experiments were conducted from which the initial five experiments spanned approximately the ambient CO_2 range (340 to 440 µmol mol^{-1}). The later experiments used spiked CO_2 concentrations in order to investigate a wider CO_2 concentration range. Figure 6 displays results for both ranges of the CO_2 cross-sensitivity for N_2O. Both experiments are in accordance with each other, although they were performed several months apart. However, the wider CO_2 range reveals further details about the shape of the CO_2 cross sensitivity for N_2O. The wide range of the CO_2 cross-sensitivity can be adequately described by a cubic relation, with a correlation coefficient $r^2 > 0.99$. The typical range of unpolluted ambient air (370 to 420 µmol mol^{-1}) can be approximated linearly with less than 0.05 nmol mol^{-1} N_2O deviation. However, for larger CO_2 values the deviation between the two approximations becomes substantial.

The CO_2 cross-sensitivities for CO and $\delta^{13}CO_2$ in the wider range of CO_2 are also not linear. Similar to the case for N_2O, the cross-sensitivities for both species can be approximated linearly in the unpolluted CO_2 range. For CO the CO_2 cross-sensitivity starts deviating significantly from a linear relation for CO_2 values above 500 µmol mol^{-1}. In Table 1 the magnitude of the CO_2 cross-sensitivities are summarised for the linearly approximated unpolluted CO_2 range. $\delta^{13}CO_2$ actually depends inversely on CO_2 and is dealt with explicitly in Griffith et al. (2012). For N_2O and $\delta^{13}CO_2$ the effect of the CO_2 cross-sensitivity is by far larger than the ILC targets, whereas for CO as well as for CH_4 the CO_2 cross sensitivity is smaller. The Heidelberg FTIR data post-processing includes the non-linear CO_2 cross sensitivity corrections for all species, also in the linear range. The sensitivity of N_2O to CO_2 could be improved by a different selection of spectral region for analysis to minimise overlap; this approach is under investigation and yields promising first results.

AMTD
5, 3645–3692, 2012

4 Instrument response function

As the supposedly *absolute* mole fraction determination of the in-situ FTIR analyser differs from the internationally accepted WMO scales by up to a few percent, depending on species (Griffith et al., 2010), calibration of the FTIR analyser with internationally accepted standard reference material is necessary to achieve the required accuracy and comparability for ambient air monitoring. The shape of the instrument response function (IRF) determines the number of required calibration standards. To determine the IRF of the in-situ FTIR analyser we analysed our set of primary laboratory standards calibrated by the WMO Central Calibration Labs (CCL). We have 13 primary laboratory standards which have been calibrated for CO_2 on the X2007 mole fraction scale. Seven, respectively five of these cylinders have also been calibrated for N_2O and CH_4 by NOAA/ESRL which also acts as the WMO-GAW Central Calibration Laboratory (CCL) for these trace gases. For $\delta^{13}CO_2$, in the course of the ICOS demo-experiment, we received four reference standards which were calibrated on the VBDP/j-RAS06 scale by the Max-Planck Institute for Biogeochemistry (MPI-BGC) in Jena, being the WMO-GAW Central Calibration Lab for stable isotopes in CO_2. The same cylinders were calibrated for the CO mole fractions by the MPI-BGC GasLab on the NOAA/ESRL 2004 scale. The calibrated range for each species is given in Fig. 7 and its caption.

All FTIR measurements of these calibration cylinders were corrected for residual- and cross-sensitivities as described in the previous section; measurements were performed on three consecutive days. Linear regression of the sensitivity-corrected FTIR mole fractions against the assigned cylinder reference values showed no significant curvature but there was a significant non-zero intercept. In Fig. 7 the residuals to the linear fit confirm that the assumption of linear instrument response functions is justified for all species. The error bars in Fig. 7 depict the combined error of the FTIR measurement and the error of the calibration cylinder assigned mole fractions. The standard deviations of the residuals are 0.03 µmol mol^{-1} for CO_2, 0.04 ‰ for $\delta^{13}CO_2$, 0.4 nmol mol^{-1} for CO, 0.4 nmol mol^{-1} for CH_4 and 0.08 nmol mol^{-1} for N_2O. From these results we

AMTD
5, 3645–3692, 2012

can conclude that the IRFs are linear over the investigated range for all tracers. However, the non-zero intercepts of the regression functions prevent a simple one point calibration, leading to a minimum of two calibration standards for the FTIR.

5 Temporal stability of the FTIR analyser and calibration frequency

In order to assess the precision of the in-situ FTIR analyser, measurement repeatability as well as reproducibility on different time scales has to be determined. In the following, we will use the terminology related to the GAW Glossary of QA/QC (Klausen and Scheel, 2007). The issue of measurement stability is vital for all long-term monitoring efforts and determines the required calibration frequency to reach a certain level of reproducibility. In the following we will subdivide the stability requirement into two parts; short-term and long-term. "Short term" handles drifts and other artefacts on a time scale from hours to days, while "long-term" covers weeks to months.

5.1 Short-term stability

To quantify short-term drifts of the FTIR analyser, a target gas was continuously flushed through the cell at the standard flow rate of 1 slpm for six days, comprising a weekend as well as weekdays, to cover different laboratory conditions. Absorption spectra with an averaging time of one minute were recorded and analysed offline to avoid down time. The respective time series of the dry air mole fractions, calculated according to Eq. (2), are shown in Fig. 8 in grey. The sensitivity corrected results are shown as well (coloured symbols).

This short-term stability test was conducted in September 2011 after the installation of the mass flow controller after the cell (see Sect. 2). Thus, the sample properties in the cell remained fairly constant over the course of the experiment as expressed by their 1σ standard deviations: $\pm 0.01\,^{\circ}\mathrm{C}$ for cell temperature, ± 0.01 hPa for cell pressure, $\pm 0.2\,\mu\mathrm{mol\,mol}^{-1}$ for moisture level, and ± 0.01 slpm for sample flow-rate. Although our

AMTD
5, 3645–3692, 2012

laboratory is air-conditioned, the temperature oscillated between 23.2 °C and 25.1 °C. However, this did not have a large influence on cell temperature and the very stable sample properties in the cell lead to only small corrections of the residual sensitivities (Fig. 8). For CO_2, a clear correlation to room and thus cell temperature was found. The sensitivity corrections thus improve the CO_2 standard deviation of the minutely measurements from 0.037 to 0.029 µmol mol^{-1}, for all other species the sensitivity corrections are marginal.

The initial 6 h of the test show a small settling-in effect for CO_2 as well as for CO which most likely can be attributed to adjustments of the pressure-regulator of the cylinder and the cell parameters. $\delta^{13}CO_2$ and CH_4 show a slight trend over the six days, persisting even after the sensitivity correction. However the drift rate is 0.02 ‰ day^{-1} for $\delta^{13}CO_2$ and −0.04 nmol mol^{-1} day^{-1} for CH_4. The drift in $\delta^{13}CO_2$ might be related to a fractionation effect in the fast emptying high pressure cylinder, however, this cannot be proven since no pre and post mass spectrometer measurements have been performed on this cylinder.

The same dataset from September 2011 (Fig. 8) can be used to determine the repeatability of the FTIR measurements using Allan variance analysis (Werle et al., 1993). In Table 2, the 1σ repeatability for 2.5 and 10 min averaging time is given. 2.5 min averaging time is used in standard operating conditions for the Heidelberg in-situ FTIR (3 min measurements including 30 s online analysis time). This time step was chosen as a trade off between instrument precision and detectable ambient variability. For example, in Heidelberg, CO values can change by more than 100 nmol mol^{-1} within 30 min during a rush-hour situation (Hammer et al., 2009), which we would like to resolve with the instrument. The 10 min repeatability is given for reasons of comparability to the earlier results from Griffith et al. (2010, 2012). Similar to the findings by Griffith et al. (2010, 2012), the repeatability of all species except for CO_2 initially improves with the square root of averaging time, although in our experiments this is only valid for the first 40 min and not for 1–2 h as found by Griffith et al. (2010, 2012). For longer integration intervals the repeatability still improves, but at a slightly lower rate.

AMTD
5, 3645–3692, 2012

For sensitivity-corrected CO_2, the repeatability improves steadily up to an averaging time of 15 h but only by one third of the square root of time.

We determined the reproducibility for measurements averaged over three minutes, as given in Table 2, by pooling three one minute spectra and calculated their 1σ standard deviation. This reproducibility includes any potential changes or arbitrary drifts in the spectrometer or any sensor over the investigated six days period. The comparison of the repeatability and reproducibility of the three minute averages in Table 2 emphasises the remarkably good short term stability of the in-situ FTIR.

5.2 Long-term stability of the in-situ FTIR analyser

The long-term stability of the instrument response function (IRF) determines the calibration frequency as well as the calibration strategy. If the IRF is absolutely stable in time, interpolation between repeated calibrations does not improve measurement accuracy. This is due to the intrinsic uncertainty of each calibration measurement which is then passed on to the measurements and increases their noise. If, on the other hand, the temporal changes of the IRF are larger than the instrument's repeatability, regular calibration improves the accuracy substantially. In the latter case the question about the calibration frequency arises. In Sect. 5.1 we showed that, compared to the noise, for CO_2, CO and N_2O, no systematic change of residual pressure and temperature sensitivity-corrected data occurred over the timescale of up to six days. Here we will investigate the longer time scales, based on the data set we collected during the ICOS demo-experiment. During these field campaigns, daily to two-daily calibrations were performed with two standard cylinders, covering a suitable mole fraction range for all five components. In between the calibrations, a so-called target tank was measured for quality control. In terms of sensitivity correction and calibration the target cylinder was analysed in a similar way as to any unknown sample from a cylinder. In the next sub section we will revisit the influence of the residual- and cross sensitivities discussed in Sect. 3 on the example of the CO_2 long-term target record.

AMTD
5, 3645–3692, 2012

5.2.1 Influence of the CO_2 residual- and cross-sensitivities on long-term records

Figure 9 displays the deviations of the CO_2 target measurement from the mean mole fraction over the different evaluation stages from the raw FTIR measurements to the finally calibrated data. Each target gas value consists of the average and the standard deviation of five sequentially recorded three minute spectra. The dry-air mole fractions as calculated by MALT are shown in blue; they exhibit step-changes as well as gradual changes. The 1σ standard deviation for the CO_2 target gas is 0.25 µmol mol^{-1} with a peak to peak variability of 0.8 µmol mol^{-1} over the five month measurement period. The prominent changes in the dry-air mole fraction can be related to changes in cell temperature and pressure, caused by changing laboratory conditions and/or a degradation of the flow controller which was additionally installed during the ICOS demo-experiment. Correction for residual- and cross-sensitivities determined in Sect. 3 improves the reproducibility of the daily to two daily values as well as the 1σ scatter over the whole period by a factor of two to only 0.11 µmol mol^{-1} (red dots in Fig. 9). The residual- and cross-sensitivity correction takes care of most of the pronounced step changes, however some outliers are persistent (e.g. in mid of July) and can thus not be explained by a change in one of our investigated residual- and cross-sensitivities. The variability in the sensitivity corrected target gas measurements is still larger than the observed short term repeatability expressed by the error bars and investigated in Sect. 3. In addition, the CO_2 variability still shows long-term changes and outliers. Thus, applying regular, e.g. daily calibration might help reducing the CO_2 variability further. By using a linear interpolation between the daily to two daily calibration measurements to determine the IRF, the 1σ standard deviation of the CO_2 target measurements is reduced to 0.05 µmol mol^{-1} as shown by black squares in Fig. 9.

Although the calibrated measurements generally satisfy the WMO compatibility goals of ±0.1 µmol mol^{-1} for CO_2 measurements in the Northern Hemisphere, individual measurement periods show greater scatter (e.g. in July). One outlier appeared due

AMTD
5, 3645–3692, 2012

to a wrong calibration measurement. The impact of a single calibration measurement depends largely on the strategy chosen to derive the IRF. We therefore investigated different calibration strategies such as (a) averaged IRF, (b) interpolated IRF between smoothed calibration measurements and (c) interpolated IRF between neighbouring calibration measurements. Based on the repeatability of the target cylinder measurements, strategy (c) yielded the best results, although its sensitivity to single outliers in the calibration measurements is largest. Careful selection of calibration outliers is thus recommended to minimise artefacts in the time series.

5.2.2 Long term reproducibility for all species

Figure 10 comprises the sensitivity-corrected and calibrated target gas measurements for all components. In September 2011 the FTIR system was modified and the respective changes and improvement are discussed in Sect. 6. The long-term reproducibility of the original FTIR set-up can be judged based on the 1σ standard deviations up to September 2011: 0.06 µmol mol^{-1} for CO_2, 0.05 ‰ for $\delta^{13}CO_2$, 0.45 nmol mol^{-1} for CO, 0.28 nmol mol^{-1} for CH_4 and 0.1 nmol mol^{-1} for N_2O. Thus, the achieved scatter is close to or within the ILC targets for all trace gases (WMO, 2011). For $\delta^{13}CO_2$ the reproducibility of 0.05 ‰ is acceptable, keeping in mind that the in-situ FTIR analyser is one of the first instruments delivering continuous $\delta^{13}CO_2$ measurements. The WMO-GAW requested target compatibility is 0.01 ‰, and yet only met by very few mass spectrometer laboratories (Huang et al., 2011).

No significant drift was observed for any species. The small step change in CO is not explained by any of the investigated sensitivities. Recalibration of the working standards as well as the target tank at MPI-BGC in Jena confirmed that neither the target cylinder nor the calibration cylinders drifted in any of the investigated species.

For CO_2 it is obvious that the performance of the in-situ FTIR analyser declined after mid of June 2011. Checking the FTIR parameters revealed that from mid of June onwards the standard deviation of the sample pressure increased from better than 2 hPa

AMTD
5, 3645–3692, 2012

to more than 7 hPa. This increase was most likely caused by a progressive degradation of the additionally installed external mass flow controller (blue MFC in Fig. 1). In Sect. 3 we have shown that the largest pressure sensitivity corrections are found for CO_2, consequently we observe the largest deviation between the short- and long-term reproducibility for CO_2. The decrease in reproducibility for CO is caused by the step change and for N_2O by several outliers. Short- and long-term reproducibility are comparable for $\delta^{13}CO_2$ and CH_4. These results demonstrate that even under varying laboratory conditions, the long-term stability of the in-situ FTIR analyser is suitable for background air monitoring if measurements are calibrated and properly corrected for residual and cross sensitivities.

5.3 Calibration frequency

The target gas record can further be used to estimate the influence of the calibration frequency on the reproducibility. In Fig. 10 we used the highest calibration frequency of daily to two daily calibrations with two standard gases. With the target gas data set we can investigate the influence of stepwise prolonged calibration intervals on the 1σ reproducibility of the results. Since, especially for CO_2, the performance of the FTIR analyser can be separated into two periods, stable and less stable conditions, we will evaluate the calibration frequency test for both stability conditions separately. The less stable period was caused by the malfunctioning of the additional MFC. Thus the instrument set-up is comparable to the standard UOW in-situ FTIR analyser configuration.

In each panel of Fig. 11 the relation between 1σ reproducibility and calibration frequency is plotted. Closed symbols represent stable instrument conditions with a cell pressure variability of less than 2 hPa, open symbols show less stable conditions; here, the cell pressure variability was four times larger. Under stable instrument conditions the 1σ target reproducibility of CO_2 was better than 0.03 µmol mol^{-1} for daily to two daily calibrations. Prolonging the calibration frequency even to 2 or 3 months changes the reproducibility only slightly to 0.05 µmol mol^{-1}. During less stable instrument conditions the reproducibility improves steadily with increasing calibration

AMTD
5, 3645–3692, 2012

frequency, however, even daily to two-daily calibrations do not result in the reproducibility of the stable conditions. It seems that under less stable conditions substantial variations occur on sub-daily time scales. E.g. during the campaign in OPE, the laboratory temperature changed by 10 °C within one day.

The other trace species, apart from N_2O, show a similar behaviour to CO_2, although the difference between stable and less stable instrument conditions is not as pronounced. For the highest calibration frequency the achieved reproducibility is on par or even better than the short-term reproducibility presented in Sect. 5.1. This is caused by the fact that the investigated target and calibration measurements are averaged values of five individual spectra, which reduces the scatter by a factor 2. This implies that for a single 3 min ambient air measurement the reproducibility is ≈50 % larger than the one shown for the target measurements. Different from other instrument response functions, the IRF for N_2O has two large step changes during the stable instrument conditions (not shown) leading to the inverse results in the calibration frequency investigation. The recorded sample and instrument properties give no evidence that could explain the step changes in the N_2O IRF.

Increasing the calibration frequency from weekly to daily/two-daily improves the reproducibility on average by 20 % for all gases. Depending on the specific accuracy needs, weekly calibrations might be sufficient and beneficial for calibration gas consumption as well.

6 Improvements

The experience gathered during the ICOS demo-experiment revealed that the largest source of variability was associated with changes in cell temperature and cell pressure. This led to the following modifications of the FTIR analyser which are now part of the standard instrument set-up for the in-situ FTIR analysers offered by Ecotech (Knoxfield, VIC, Australia; this company took over the instrument's commercialisation from the University of Wollongong):

AMTD
5, 3645–3692, 2012

1. The needle-valve flowmeter unit was replaced by an internal mass flow controller (Model 3660, Kofloc, Japan) (compare blue and red parts in Fig. 1). The MFC is located at the outlet of the cell and can be operated in flow control mode or in pressure control mode when combined with a feedback-loop to the pressure sensor which is embedded in the software.

2. The RTD temperature sensor in the cell was replaced by a faster J-type thermocouple to shorten the response time after evacuation of the cell, which was found to be in part an artefact of the RTD sensor, caused by its large thermal mass. The thermocouple was centred in the cell to get a more representative temperature measurement.

The Heidelberg in-situ FTIR analyser was equipped with these improvements in September 2011 and operated in this "Ecotech" standard configuration for two months. At the same time the additional external MFC after the selection valve (Fig. 1) was removed.

With the modified set-up, the temperature disequilibrium sensitivity for cylinder measurements was not observed anymore. Although the laboratory temperature at the IUP is fairly stable and led to a sample temperature variation of 0.1 °C only, the strong temperature disequilibrium sensitivity (TDS), as discussed in Sect. 3.4, should cause a 0.2 µmol mol^{-1} variation in CO_2 which is not observed. The observed temperature sensitivity for cylinder measurements was similar to the residual temperature sensitivity found in the dedicated temperature experiments discussed in Sect. 3.3. This points towards a relation between the TDS and the formerly used RTD sensor.

The first red shaded area in Fig. 10 marks the re-building period which was followed by standard operation of the in-situ FTIR analyser comprising daily target gas measurements and calibrations. The reproducibility derived with this instrument configuration is given in Table 2. The largest improvement compared to the original set-up, a factor of 2, was achieved for N_2O, improving the in-situ FTIR analyser precision to well below the ILC target. The performance for CO_2, $\delta^{13}CO_2$ and CH_4 remains at a comparably

AMTD
5, 3645–3692, 2012

good level. The drift which was observed for CO was caused by a drifting calibration gas cylinder being used during this time. Uncalibrated results suggest that the CO reproducibility improved as well.

The sample pressure stabilisation using the MFC in combination with a feedback loop to the cell pressure sensor is accurate to better than 0.1 hPa deviation. However, changes in delivery pressure are compensated for by flow-rate variations. In Sect. 3.5 we have shown that the flow-rate sensitivities are small and thus do not hinder this approach. However, for precious calibration gas where as little as possible should be used, this implies special care when tuning the pressure regulator, otherwise more gas than needed would be used caused by the higher flow-rate.

To decouple sample pressure and flow, and to ease sample handling, we installed an additional electronic pressure controller (EPC) (El-Press, Bronkhorst, The Netherlands) at the inlet of the cell. In Fig. 10 the target gas measurements performed with this new configuration are shown after the second red shaded area. The reproducibility of the sensitivity-corrected and -calibrated target gas results is also summarised in Table 2. The introduction of the additional EPC improved the reproducibility of all components apart from N_2O by approximately a factor of two. The dashed line in Fig. 10 in mid December 2011 indicates a change in our standard operation conditions. From there on we skipped the evacuation step during sample exchange and used the flushing approach (compare Sect. 2.4). This was done in order to investigate the benefits of not disrupting the temperature and moisture equilibrium in the cell by the evacuation. In Fig. 10 no significant difference between both sample change-over strategies is visible. Thus after two months we changed back to our SOC to save calibration gas and to shorten the calibration measurements.

7 Error assessment for ambient air measurement

Different sources of error contribute to the total error of an individual ambient air measurement. These error contributions are partly systematic and partly random and can

AMTD
5, 3645–3692, 2012

often not easily be separated. Obvious error contribution arises from: (a) measurement repeatability, (b) uncertainties in residual- and cross-sensitivity corrections, (c) uncertainties introduced by the two-point calibration and (d) uncertainty of the assigned mole fraction of the calibration cylinders themselves.

These error sources are not independent from each other. For example, the uncertainties originating from (a) and (b) (repeatability and the residual- and cross-sensitivity corrections) feed directly into the uncertainty introduced by the regular calibration. Thus a combined uncertainty comprising (a), (b) and (c) can be derived from the reproducibility of the target measurements as listed in Table 2. However, the target measurement reproducibility is derived from averaged values and has thus to be multiplied by 2. For ambient air measurements the uncertainties of the CO_2 cross-sensitivities must be added since this error component is not present in the target measurements. The total uncertainties are thus given in the last column of Table 2. The contribution of the uncertainties of the assigned values of the calibration cylinders is an additional, systematic error component which has to be accounted separately.

8 Conclusions and outlook

The Wollongong FTIR spectrometer is well suited for atmospheric GHG monitoring and fulfils the precision, accuracy and stability needs for CO_2, CO, CH_4 and N_2O measurements at background sites. The reproducibility for $\delta^{13}CO_2$ does formally not fulfil the ILC targets set by WMO-GAW; however, 0.03 ‰ target reproducibility (0.07 ‰ single measurement) is still very good for a continuously measuring instrument. In the final configuration, including the internal EPC and MFC to control the sample properties in the cell, the effects of the residual pressure sensitivity and flow rate-sensitivity are negligible. The same is true for the H_2O cross-sensitivity, since the residual moisture variations can be restricted to a few µmol mol^{-1} of H_2O, only. Reducing the causes of variability is always superior to any post-processing correction. However, for those parameters where this is not possible, e.g. CO_2, precise determination of cross-sensitivities

AMTD
5, 3645–3692, 2012

is essential. Currently, the largest remaining issues are related to residual sample temperature sensitivity, and thus to the ability of measuring the mean sample temperature in the cell. Although we did not observe the strong TDS for cylinder measurements after replacement of the RTD sensor, further investigation is needed. The small Reynolds number in the cell (≈10) for our standard operating conditions constitutes a more general problem. Improved sample delivery to the cell which increases turbulence would help minimizing temperature gradients within the cell. Alternatively, measuring the sample temperature at multiple locations would improve the representativeness of the temperature measurement as well. We also recommend placing the Nafion drier inside the temperature controlled enclosure, since it is important for thermal sample preconditioning.

The instrument has proven to be acceptably linear for all components in the ambient concentration range (also for non background conditions), however, the instrument response functions have a non zero offset for all components implying the need of at least two calibration gases. The in-situ FTIR analyser is sufficiently stable to run with only weekly calibrations. In standard operation conditions 30 l of air are needed for one calibration measurement. Thus, a 50 l cylinder pressurised to 20 MPa lasts for more than four years, even if 10 % to 20 % of the gas is left over to avoid potential drifts in the cylinders (Kitzis, 2009; Langenfelds et al., 2005). For conservative, high accuracy applications, one may want to have a full year of overlap between two calibration gas generations resulting in an effective calibration gas life time of three years. For high accuracy applications we recommend to use three calibration cylinders spanning the range of expected ambient concentrations. The usage of three calibration gases instead of the minimally needed two reduces the sensitivity to individual outliers and instrument noise. In any case we recommend daily target gas measurement for quality control. The lifetime of a daily target gas is unfortunately limited to nine months only, thus we recommend a second sub-target being measured on a two weekly basis only. The sub-target can then also be used to inter-connect two to three standard gas generations.

AMTD
5, 3645–3692, 2012

Acknowledgements. Martin Riggenback and Graham Kettlewell are gratefully acknowledged for building and improving the hardware and software of the in-situ FTIR analyser and for many hours of sharing ideas with the authors. We are very grateful to Armin Jordan and Bert Steinberg for the preparation and careful calibration of the high pressure cylinders used during the ICOS demo-experiment. We wish to thank Alex Vermeulen (ECN) and the team from KNMI for hosting us at Cabauw tower, and Sébastien Connil (Andra) and Marc Delmotte (LSCE) for the support at OPE. This work has been funded by the European Commission under the ICOS Preparatory Phase Project (INFRA-2007-211574) and additionally supported by the "Global Networks" program of the Heidelberg University, and International Science Linkages/Europe Fund grant (EF-090007) and Australian Research Council Discovery Grant (DP0879468) from the Australian Government.

References

Chen, H., Winderlich, J., Gerbig, C., Hoefer, A., Rella, C. W., Crosson, E. R., Van Pelt, A. D., Steinbach, J., Kolle, O., Beck, V., Daube, B. C., Gottlieb, E. W., Chow, V. Y., Santoni, G. W., and Wofsy, S. C.: High-accuracy continuous airborne measurements of greenhouse gases (CO_2 and CH_4) using the cavity ring-down spectroscopy (CRDS) technique, Atmos. Meas. Tech., 3, 375–386, doi:10.5194/amt-3-375-2010, 2010.

Esler, M. B., Griffith, D. W. T., Wilson, S. R., and Steele, L. P.: Precision trace gas analysis by FT-IR spectroscopy 1. simultaneous analysis of CO_2, CH_4, N_2O and CO in air, Anal. Chem., 72, 206–215, 2000a.

Esler, M. B., Griffith, D. W. T., Wilson, S. R., and Steele, L. P.: Precision trace gas analysis by FT-IR spectroscopy 2. the $^{13}C/^{12}C$ isotope ratio of CO_2, Anal. Chem., 72, 216–221, 2000b.

Francey, R. J. and Steele, L. P.: Measuring atmospheric carbon dioxide – the calibration challenge, Accredit. Qual. Assur., 8, 200–204, 2003.

Glatzel-Mattheier, H.: Bilanzierung von CH_4-Emissionen in Deutschland anhand atmosphärischer Messungen in Heidelberg, PhD thesis, University of Heidelberg, Germany, 129 pp., 1997.

Griffith, D. W. T.: Synthetic calibration and quantitative analysis of gas phase infrared spectra, Appl. Spectrosc., 50, 59–70, 1996.

AMTD

5, 3645–3692, 2012

Griffith, D. W. T., Deutscher, N. M., Krummel, P., Fraser, P., van der Schoot, M., and Allison, C.: The UOW FTIR trace gas analyser: comparison with loflo, agage and tank measurements at Cape Grim and gaslab, Baseline Atmospheric Program, Australia, 2010.

Griffith, D. W. T., Deutscher, N. M., Caldow, C., Kettlewell, G., Riggenback, M., and Hammer, S.: A Fourier Transform Infrared trace gas analyser for atmospheric applications, Atmos. Meas. Tech., submitted, 2012.

Hammer, S.: Quantification of the regional H_2 sources and sinks inferred from atmospheric trace gas variability, PhD thesis, University of Heidelberg, Germany, 121 pp., 2008.

Hammer, S., Vogel, F., Kaul, M., and Levin, I.: The H_2/CO ratio of emissions from combustion sources: comparison of top-down with bottom-up measurements in the Rhine-Neckar region in Southwest Germany, Tellus B, 61, 547–555, doi:10.1111/j.1600-0889.2009.00418.x, 2009.

Huang, L., Chivulescu, A., Allison, C., Brailsford, G., Brand, W. A., Wendeberg, M., Bollenbacher, A., Keeling, R., Levin, I., Sabasch, M., Leuenberger, M., Mukai, H., Nakazawa, T., Aoki, S., Neubert, R., Aerts-Bijma, A., Verkouteren, M., White, J., Vaughn, B., Michel, S., Zhou, L., and Liu, L. X.: A report of δ^{13}C & δ^{18}O Measurements in NBS 19 and NBS 18 pure CO_2: uncertainty in traceability of CO_2 isotope measurements, in: Proceedings of the 15th IAEA/WMO meeting of CO_2 experts, Jena, September 2009, WMO-GAW Report 194, edited by: Jordan, A. and Brand, W. A., 169–175, 2011.

Keeling, C. D., Bacastow, R. B., Bainbridge, A. E., Ekdahl, C. A., Guenther, P. R., Waterman, L. S., and Chin, J. F. S.: Atmospheric carbon dioxide variations at Mauna Loa Observatory, Hawaii, Tellus, 28, 538–551, 1976.

Kitzis, D.: Preparation and stability of standard reference air mixtures, available at: http://www.esrl.noaa.gov/gmd/ccl/airstandard.html (last access: 1 February 2012), 2009.

Klausen, J. and Scheel, H.-E.: WMO/GAW glossary of QA/QC-related terminology, available at: http://gaw.empa.ch/glossary/glossary.html (last access: 16 May 2012), 2007.

Krystek, M. and Anton, M.: A weighted total least-squares algorithm for fitting a straight line, Meas. Sci. Technol., 18, 3438–3442, 2007.

Langenfelds, R. L., van der Schoot, M. V., Francey, R. J., and Steele, L. P.: Modification of air standard composition by diffusive and surface processes, J. Geophys. Res., 110, D13307, doi:10.1029/2004JD005482, 2005.

Long, D., Bielska, K., Lisak, D., Havey, D. K., Okumura, M., Miller, C. E., and Hodges J. T.: The air-broadened, near-infrared CO_2 line shape in the spectrally isolated regime: evidence

AMTD
5, 3645–3692, 2012

of simultaneous Dicke narrowing and speed dependence, J. Chem. Phys., 135, 064308, doi:10.1063/1.3624527, 2011.
Messager, C., Schmidt, M., Ramonet, M., Bousquet, P., Simmonds, P., Manning, A., Kazan, V., Spain, G., Jennings, S. G., and Ciais, P.: Ten years of CO_2, CH_4, CO and N_2O fluxes over Western Europe inferred from atmospheric measurements at Mace Head, Ireland, Atmos. Chem. Phys. Discuss., 8, 1191–1237, doi:10.5194/acpd-8-1191-2008, 2008.
Nakamichi, S., Kawaguchi, Y., Fukuda, H., Enami, S., Hashimoto, S., Kawasaki, M., Umekawa, T., Morino, I., Suto, H., and Inoue, G.: Buffer-gas pressure broadening for the (3 00 1)III ← (0 0 0) band of CO_2 measured with continuous-wave cavity ring-down spectroscopy, Phys. Chem. Chem. Phys., 8, 364–368, doi:10.1039/B511772K, 2006.
Rothman, L. S., Jacquemart, D., Barbe, A., Chris Benner, D., Birk, M., Brown, L. R., Carleer, M. R., Chackerian Jr., C., Chance, K., Couderth, L. H., Dana, V., Devi, V. M., Flaud, J.-M., Gamache, R. R., Goldman, A., Hartmann, J.-M., Jucks, K. W., Maki, A. G., Mandin, J.-Y., Massie, S. T., Orphal, J., Perrin, A., Rinsland, C. P., Smith, M. A. H., Tennyson, J., Tolchenov, R. N., Toth, R. A., Vander Auwera, J., Varanasi, P., and Wagner, G.: The HITRAN 2004 molecular spectroscopic database, J. Quant. Spectrosc. Ra., 96, 139–204, 2005.
Werle, P., Muecke, R., and Slemr, F.: The limits of signal averaging in trace gas monitoring by tunable diode laser absorption spectroscopy (TDLAS), Appl. Phys., B57, 131–139, 1993.
Winderlich, J., Chen, H., Gerbig, C., Seifert, T., Kolle, O., Lavrič, J. V., Kaiser, C., Höfer, A., and Heimann, M.: Continuous low-maintenance CO_2/CH_4/H_2O measurements at the Zotino Tall Tower Observatory (ZOTTO) in Central Siberia, Atmos. Meas. Tech., 3, 1113–1128, doi:10.5194/amt-3-1113-2010, 2010.
WMO: Report of the WMO/UNEP/ICSU Meeting on Instruments, Standardization and Measurements Techniques for Atmospheric CO_2, Geneva, 8–11 September, 1981.
WMO: Report of the 15th WMO/IAEA Meeting of Experts on Carbon Dioxide, Other Greenhouse Gases, and Related Tracers Measurement Techniques, 7–10 September 2009, GAW Report No. 194, WMO TD No. 1553, available at: http://www.wmo.int/pages/prog/arep/gaw/documents/GAW_194_WMO_TD_No_1553_web_low_resol.pdf (last access: 2 February 2012), Jena, Germany, 2011.
Worthy, D. E. J.: Canadian Baseline Program, Summary of Progress to 2002, Meteorological Service of Canada, Canada, 2003.

AMTD
5, 3645–3692, 2012

Table 1. Summary of all residual- and cross-sensitivity experiments for all species. For each investigated sensitivity (except for the flow rate sensitivity) three rows are given: the first row states the averaged slopes (dy/dx) of the linear regression together with their 1σ uncertainties. The second row gives an example of the magnitude of the sensitivity for a typical range of parameter variations. The last row categorizes the temporal stability of the sensitivities over the course of one year. In case of a temporally unstable sensitivity the largest sensitivity value (dy/dx) is given as an upper estimate and in those cases no uncertainty estimates are tabulated. For the flow rate sensitivity an additional row is given stating the difference between a measurement performed at a flow rate of 1 slpm and a static measurement. For the CO_2 cross-sensitivity only the linear cross-sensitivities for unpolluted CO_2 levels are given. The last three rows summarize the temperature disequilibrium sensitivities which were derived from cylinder measurements. The bold font of some numbers is to highlight their significance relative to the WMO inter laboratory compatibility goals.

	CO_2	error	$\delta^{13}CO_2$	error	CO	error	CH_4	error	N_2O	error
	(µmol mol^{-1})		(‰)		(nmol mol^{-1})		(nmol mol^{-1})		(nmol mol^{-1})	
dx/dp (hPa^{-1})	0.0085	0.0004	0.005	0.002	0.006	0.002	0.031	0.003	0.007	0.001
Typical variation for 20 hPa	**0.17**	0.01	**0.10**	0.04	0.12	0.04	0.62	0.06	**0.14**	0.02
Temporal development	stable		linear decreasing		stable		linear decreasing		stable	
dx/dT (°C^{-1})	< 0.8	–	0.6	0.2	< 1	–	< 1.6	–	0.6	0.2
Typical variation for 0.1 °C	< 0.08	–	**0.06**	0.02	0.10	–	0.16	–	0.06	0.02
Temporal development	unstable		rel. stable		unstable		unstable		rel. stable	
dx/dFlow (slpm^{-1})	0.15	0.001	−0.9	0.6	< 2	–	< 4	–	< −0.8	–
Typical variation for 0.03 slpm	0.00	0.00	**−0.03**	0.02	< 0.1	–	< 0.1	–	< −0.02	–
static vs. 1 slpm	0.25		0.60		0.10		1.40		0.28	
Temporal development	stable		unstable		unstable		unstable		unstable	
dx/dH_2O (µmol^{-1} mol (H_2O))	0.04	0.02	–	–	< 0.2	–	< 0.2	–	–	–
Typical variation for 2 µmol mol^{-1}(H_2O)	0.08	0.04	–	–	< 0.4		< 0.4	–	–	–
Temporal development	stable				unstable		unstable			
dx/dCO_2 (µmol^{-1} mol)	–	–	0.006	0.0003	< 0.015		–		0.008	0.0008
Typical variation for 50 µmol mol^{-1}(CO_2)	–	–	**0.3**	0.02	0.75		–		**0.4**	0.04
Temporal development			stable		unstable				stable	
dx/dT (TDS) (°C^{-1})	2.07	0.05	4.1	0.1	−4.6	0.3	10.2	0.3	3.2	0.1
Typical variation for 0.1 °C	**0.2**	0.01	**0.41**	0.01	0.50	0.03	1.0	0.03	**0.32**	0.01
Temporal development	stable		stable		stable		stable		stable	

AMTD
5, 3645–3692, 2012

Table 2. Repeatability (1σ) for 2.5 and 10 min averaging times deduced from Allan-Variance analysis. Reproducibility (1σ) for 3 min measurements of a single tank over a six day period and target gas reproducibility over the course of several months (compare Fig. 10). Total uncertainty for a single ambient air measurement (see Sect. 7).

Species	Repeatability (1σ)		Reproducibility (1σ)			Total uncertainty incl. errors in sensitivities (1σ)
Time period	2.5 min	10 min	Single tank 6 days 3 min	Target: Ecotech setup	Target: additional EPC	Single measurement
CO_2 (µmol mol^{-1})	0.018	0.012	0.023	0.043	0.016	0.032
$\delta^{13}CO_2$ (‰)	0.05	0.03	0.06	0.062	0.034	0.07
CH_4 (nmol mol^{-1})	0.2	0.1	0.2	0.21	0.12	0.25
CO (nmol mol^{-1})	0.2	0.1	0.2	0.26	0.11	0.30
N_2O (nmol mol^{-1})	0.07	0.04	0.07	0.042	0.042	0.084

AMTD
5, 3645–3692, 2012

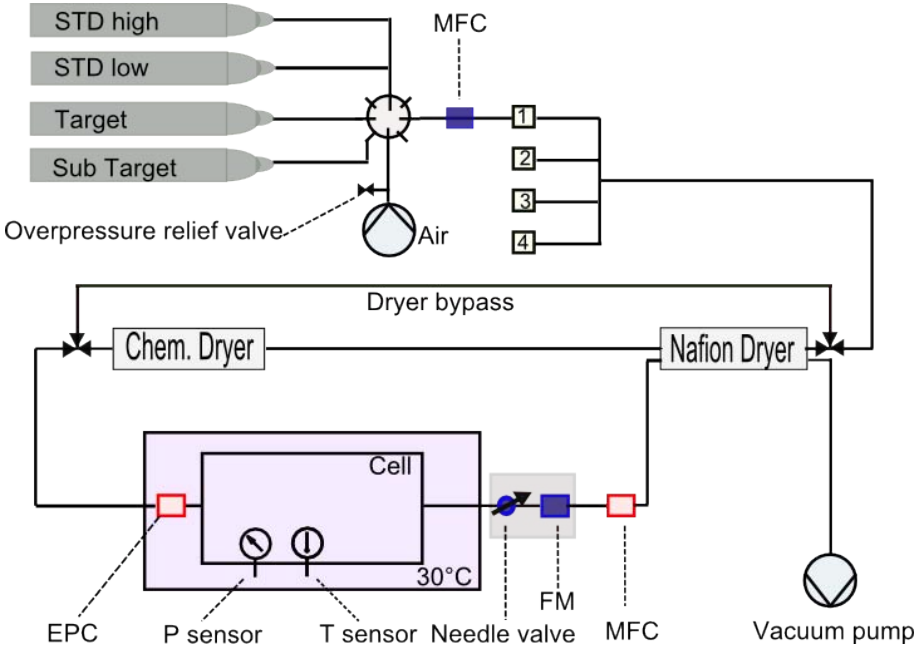

Fig. 1. Schematic set-up of the in-situ FTIR analyser. The blue parts have been replaced with the red parts in the final set-up.

AMTD
5, 3645–3692, 2012

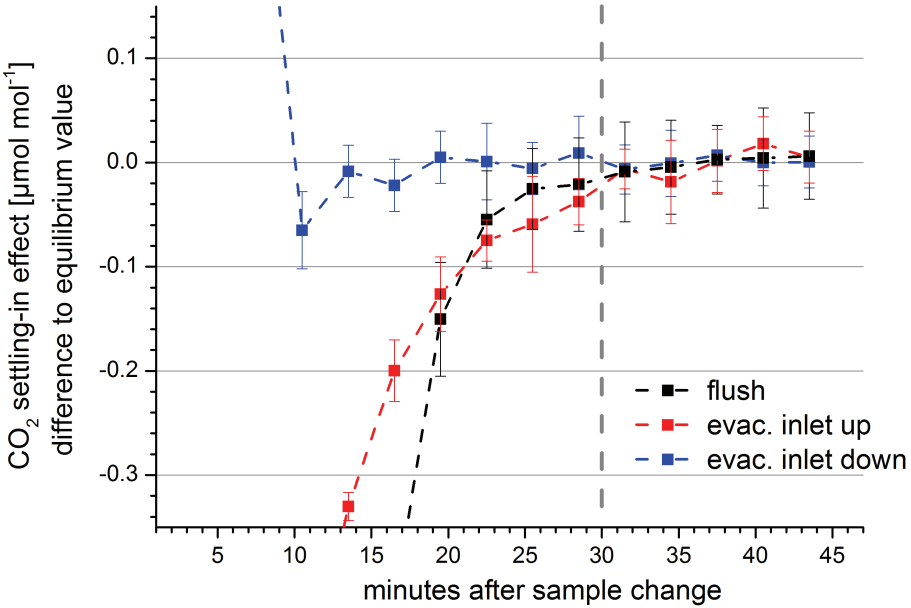

Fig. 2. Comparison of the different sample change-over methods for CO_2. The settling-in effects are shown as relative deviation from the equilibrium value defined by the average of the last five measurements. Sample exchange by flushing only is shown in black, sample exchange via evacuation under SOC in blue with standard cell orientation and in red with the cell turned upside down. Measurements are shown centred in their 3 min interval.

AMTD
5, 3645–3692, 2012

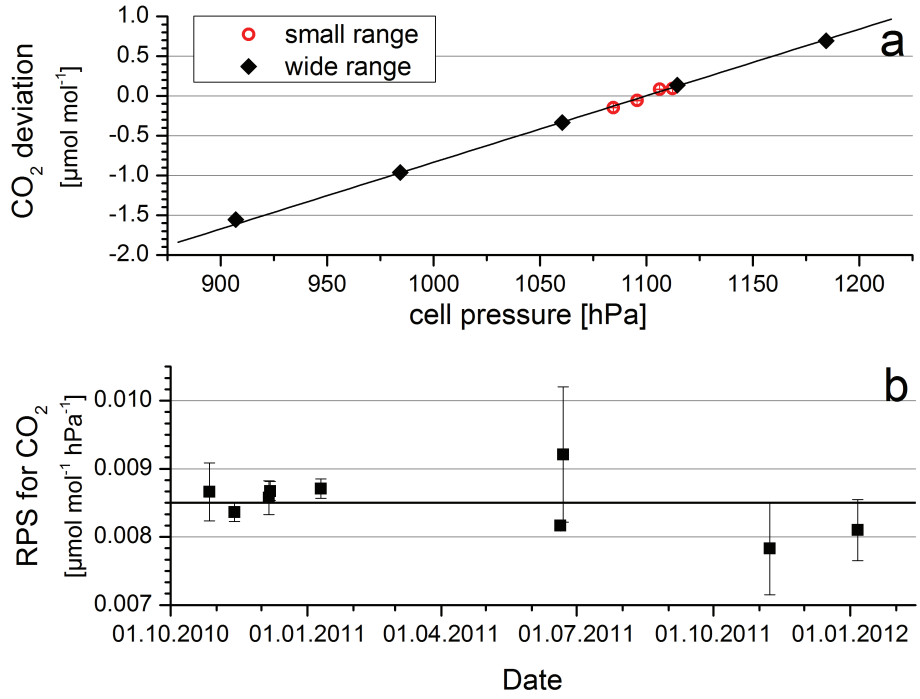

Fig. 3. (a) Residual pressure sensitivity for CO_2 measured on 20 and 22 June 2011. Small and wide pressure ranges are shown together with a linear fit. Individual errors are smaller than the symbols. **(b)** Temporal stability of the slope of the residual pressure sensitivity for CO_2. The mole fractions of the used cylinders were all in the ambient range of Heidelberg.

AMTD
5, 3645–3692, 2012

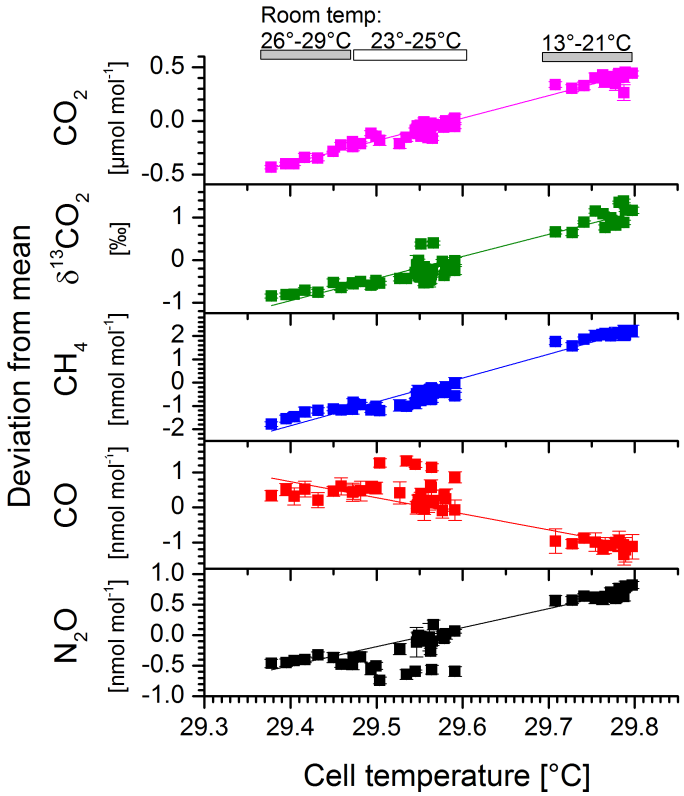

Fig. 4. Temperature disequilibrium sensitivity of the sub-target measurements, shown as deviation from mean mole fractions. Values have been corrected for all residual sensitivities except for residual temperature. The three different temperature ranges in the cell result from different laboratory temperatures at the remote (ICOS) stations and in the IUP laboratory which are indicated in the top panel.

AMTD
5, 3645–3692, 2012

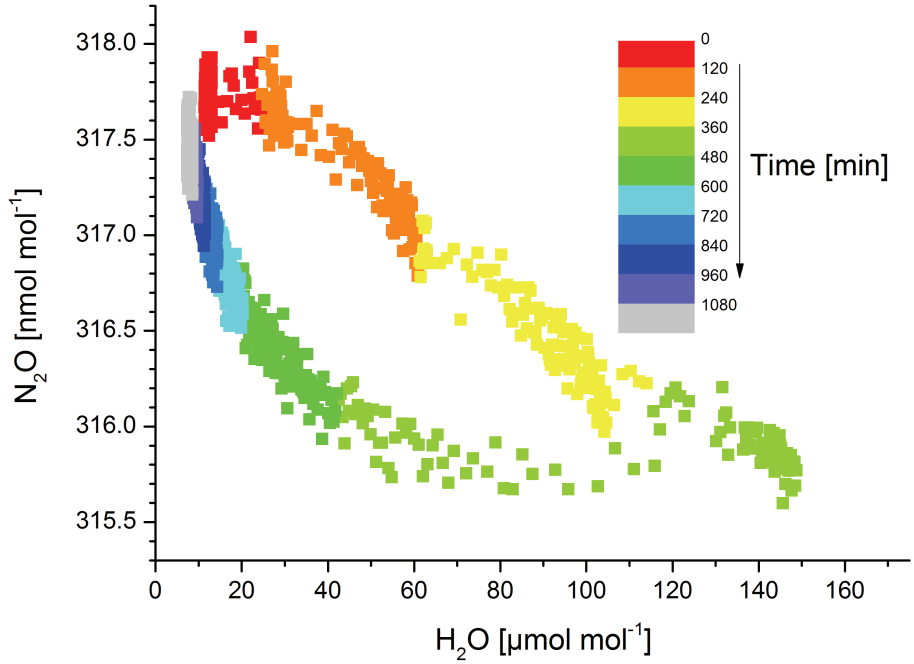

Fig. 5. H_2O cross sensitivity for N_2O. In the course of this experiment the cell was first gradually humidified and dried afterwards. The colour code represents time since start of the experiment in minutes.

AMTD
5, 3645–3692, 2012

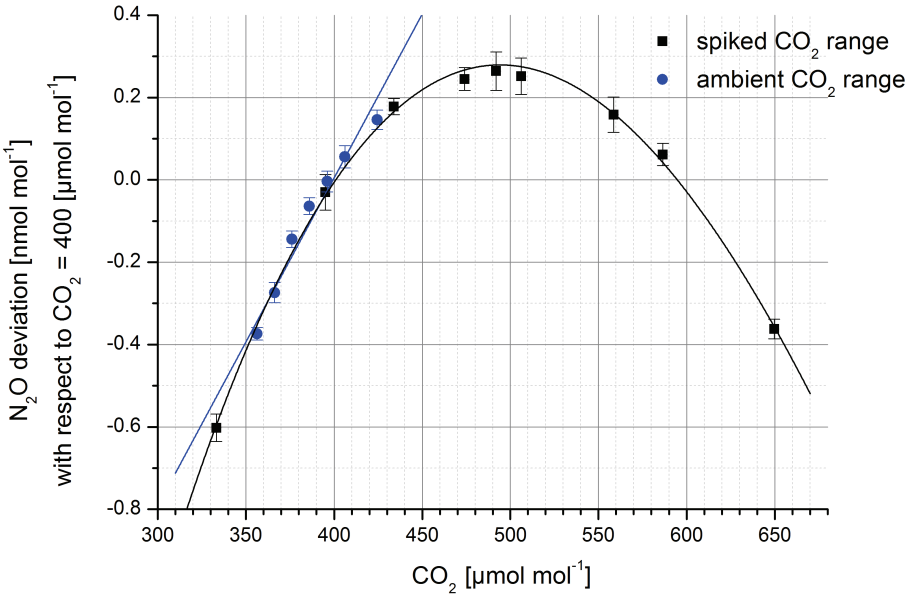

Fig. 6. CO_2 cross-sensitivity for N_2O, shown as deviation to a reference CO_2 amount of 400 µmol mol^{-1}. In blue a CO_2 cross-sensitivity experiment spanning the unpolluted CO_2 range is shown together with its linear approximation. Results from a spiked CO_2 experiment and a cubic fit are displayed in black. Both experiments have been conducted with N_2O mole fractions of about 311 nmol mol^{-1}.

AMTD
5, 3645–3692, 2012

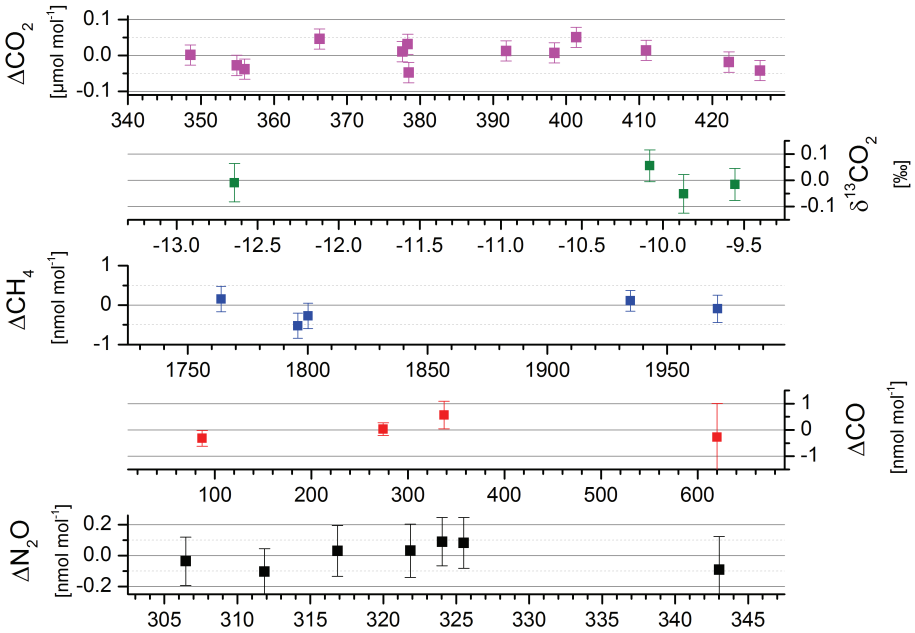

Fig. 7. Linearity of the FTIR analyser. For each species the residual to the linear fit of the externally assigned mole fractions against sensitivity corrected FTIR mole fractions are shown. The investigated mole fraction ranges are defined by the spread of our primary laboratory cylinders and are as follows: CO_2: 348 to 426 µmol mol^{-1}; $\delta^{13}CO_2$: −12.65 to −9.55‰; CO: 90 to 620 nmol mol^{-1}, CH_4: 1757 to 1970 nmol mol^{-1} and N_2O: 307 to 343 nmol mol^{-1}.

AMTD
5, 3645–3692, 2012

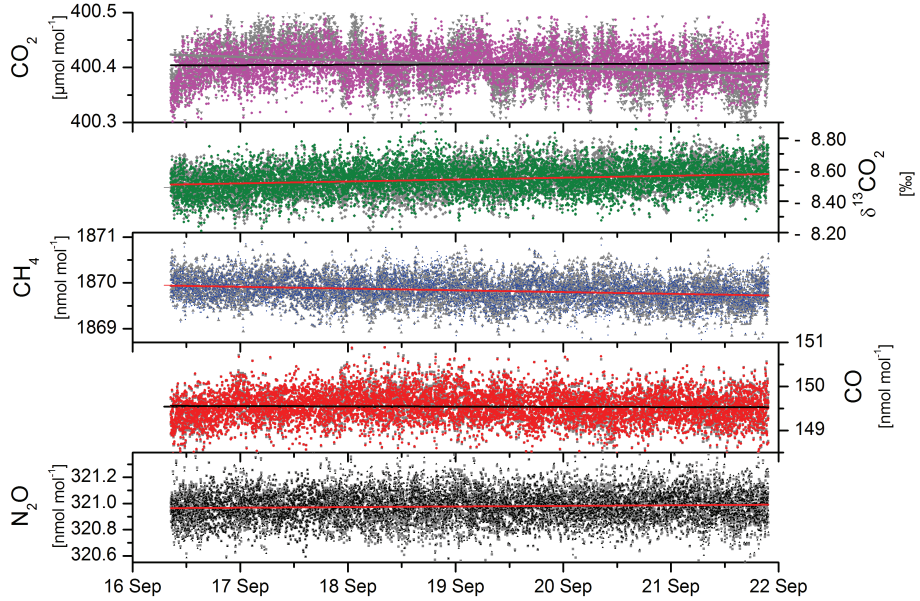

Fig. 8. Short term stability of the FTIR components during September 2011: minute-by-minute cylinder measurements over the course of six days. In grey the dry air mole fractions are given. The coloured symbols show the sensitivity corrected values, with a linear fit to detect drifts.

AMTD
5, 3645–3692, 2012

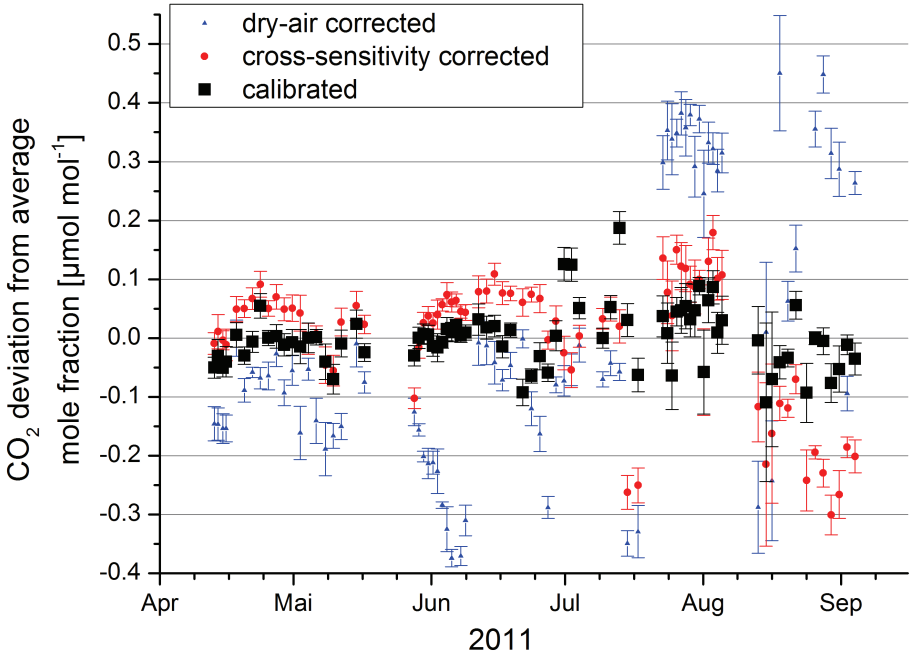

Fig. 9. CO_2 target gas record in its different data processing stages.

AMTD
5, 3645–3692, 2012

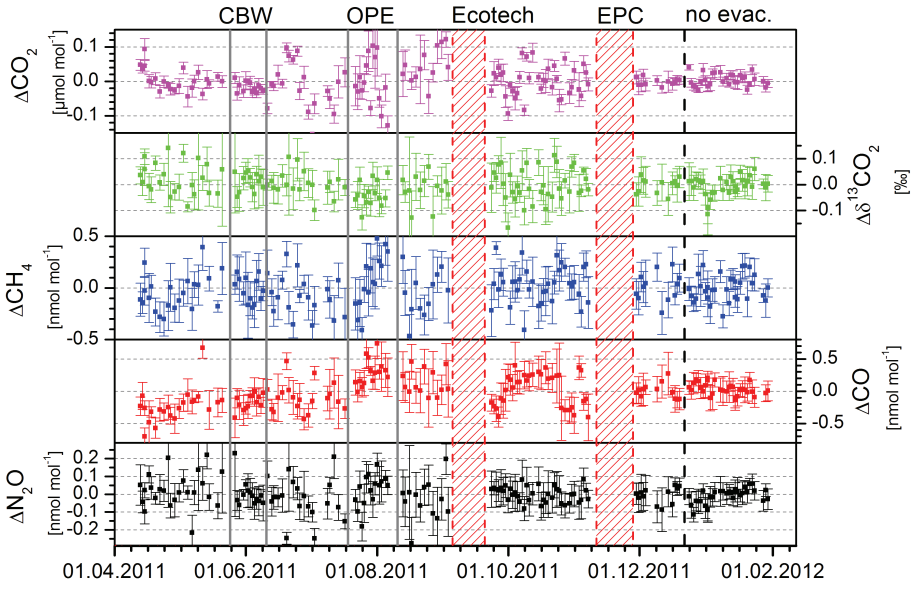

Fig. 10. Long term stability of the FTIR analyser based on the daily to two daily target gas measurements. Vertical gray lines denote location changes of the instrument. Red shaded areas mark instrument down times due to modifications and/or laser failure. In September 2011 the internal MFC and end of November 2011 the EPC was installed. The dashed black line indicates the change in SOC after which no evacuation was performed during sample exchange.

AMTD
5, 3645–3692, 2012

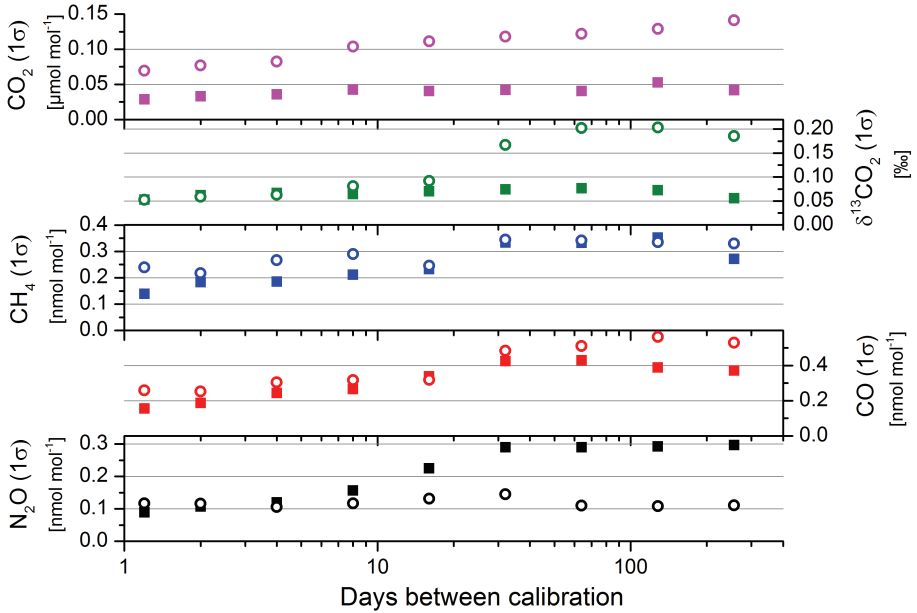

Fig. 11. Calibration frequency test. 1σ standard deviation of the target gas measurements as a function of days between calibrations. Open symbols represent less stable instrument conditions with sample pressure variations (1σ) of more than ±7 hPa. Filled symbols relate to stable conditions with sample pressure variations (1σ) of less than ±2 hPa.

AMTD
5, 3645–3692, 2012